AD-A103 948 CALSPAN ADVANCED TECHNOLOGY CENTER BUFFALO NY F/G 4/2
A FEASIBILITY STUDY OF NUMERICAL SIMULATION OF INVERSION-RISING--ETC(U)
AUG 81 C W ROGERS, J T HANLEY N00014-79-C-0459
UNCLASSIFIED CALSPAN-6512-M-2 NL

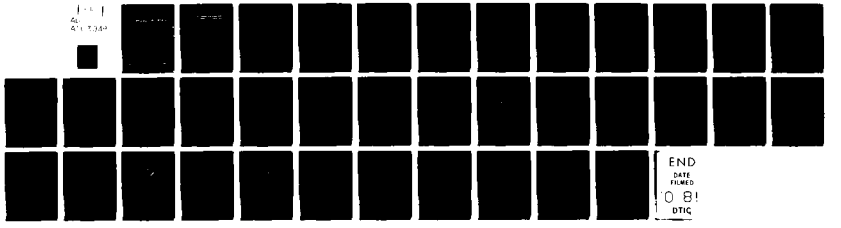

END
DATE FILMED
0 81
DTIC

LEVEL II

12

AD A103948

ARVIN/CALSPAN

ADVANCED TECHNOLOGY CENTER

DTIC
SEP 9 1981

TECHNICAL REPORT

DISTRIBUTION STATEMENT A
Approved for public release;
Distribution Unlimited

DTIC FILE COPY

BUFFALO, NEW YORK 14225
A DIVISION OF TECHNOLOGY GROUP OF ARVIN INDUSTRIES, INC.

ARVIN

81 9 08 98

12

CALSPAN ADVANCED TECHNOLOGY CENTER

A FEASIBILITY STUDY OF NUMERICAL SIMULATION OF INVERSION-RISING MARINE STRATUS AND FOG

August 1981

Calspan Report No. 6512-M-2

Contract No. N00014-79-C-0459

FINAL REPORT

DTIC ELECTE SEP 3 1981 A

By:
C. William Rogers and James T. Hanley

Prepared for:

NAVAL ENVIRONMENTAL PREDICTION RESEARCH FACILITY
MONTEREY, CA.

Through

OFFICE OF NAVAL RESEARCH
800 NORTH QUINCY STREET
ARLINGTON, VA 22217

A DIVISION OF CALSPAN CORPORATION

DISTRIBUTION STATEMENT A
Approved for public release;
Distribution Unlimited

81 9 0[illegible]

SECURITY CLASSIFICATION OF THIS PAGE (When Data Entered)

REPORT DOCUMENTATION PAGE

READ INSTRUCTIONS BEFORE COMPLETING FORM

1. REPORT NUMBER	2. GOVT ACCESSION NO. AD-A103 948
3. RECIPIENT'S CATALOG NUMBER	
4. TITLE (and Subtitle) A Feasibility Study of Numerical Simulation of Inversion-Rising Marine Stratus and Fog.	5. TYPE OF REPORT & PERIOD COVERED Final
	6. PERFORMING ORG. REPORT NUMBER 6512-M-2
7. AUTHOR(s) C. William Rogers [redacted] James T. Hanley	8. CONTRACT OR GRANT NUMBER(s) N00014-79-C-0459
9. PERFORMING ORGANIZATION NAME AND ADDRESS Calspan Corporation, PO Box 400, Buffalo, NY 14225	10. PROGRAM ELEMENT, PROJECT, TASK AREA & WORK UNIT NUMBERS
11. CONTROLLING OFFICE NAME AND ADDRESS Office of Naval Research, 800 North Quincy Street, Arlington, VA 22217	12. REPORT DATE August 1981
	13. NUMBER OF PAGES 30
14. MONITORING AGENCY NAME & ADDRESS (if different from Controlling Office)	15. SECURITY CLASS. (of this report) Unclassified
	15a. DECLASSIFICATION/DOWNGRADING SCHEDULE

16. DISTRIBUTION STATEMENT (of this Report)

Unlimited

17. DISTRIBUTION STATEMENT (of the abstract entered in Block 20, if different from Report)

18. SUPPLEMENTARY NOTES

19. KEY WORDS (Continue on reverse side if necessary and identify by block number)

Marine Fog
Numerical Simulation
Marine Inversion
California Coast

20. ABSTRACT (Continue on reverse side if necessary and identify by block number) Raising of the marine inversion above the lifting condensation level by mesoscale vertical motion associated with warm water patches can produce stratus and subsequently fog may form. The feasibility of numerical simulation of these inversion rising situations was examined. A modified numerical framework, constructed from the Lavoie model, is capable of simulating the effect of warm water patches on the formation of stratus/fog during inversion rising situations. However, the operational utility of the model is limited because the frequency of meteorological conditions during which the warm patch effect is important is very small.

DD FORM 1 JAN 73 1473 EDITION OF 1 NOV 65 IS OBSOLETE

SECURITY CLASSIFICATION OF THIS PAGE (When Data Entered)

TABLE OF CONTENTS

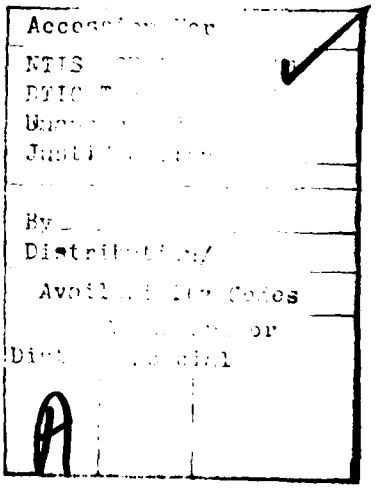

LIST OF FIGURES

LIST OF TABLES

ACKNOWLEDGMENTS

The authors would like to thank E.J. Mack, Head, Atmospheric Sciences Section, for his many helpful suggestions and criticisms during both the technical effort and the preparation of this report. We would like to express appreciation to R.J. Pilié, Head, Environmental Sciences Department, for his guidance, particularly in the treatment of cloud liquid water in the shallow marine layer.

Section 1
INTRODUCTION AND SUMMARY

Fog in the surface layer both forms in situ and arrives there from aloft. Both fog types have been numerically simulated (Oliver et al, 1978) using a higher order closure turbulence model which includes radiational transfer. In the first type, fog forms as nearly saturated air moves over warmer water. The second fog type occurs when stratus, which forms during the night from radiational cooling, subsequently lowers to the surface.

Stratus which may lower to the surface to produce fog has been observed to form by other than radiational cooling. For example, vertical motion produced by horizontal convergence associated with coastal frictional effects can produce stratus. Also, the raising of the inversion above the lifting condensation level by mesoscale vertical motion associated with warm water patches can also produce stratus. The research reported here investigated the feasibility of numerical simulation of these inversion rising fogs by use of a single, well-mixed layer model in which vertical motions occur in response to warm water patches.

The original idea to simulate inversion rising situations arose from a stratus/fog formation observed on 9 October 1976 off the California coast. In this case, clear skies occurred with an inversion located at 100 m and below the lifting condensation level (LCL). Subsequently, the inversion rose above the LCL and stratus and then fog formed. From the 1976 field study, it was suspected that warm patches of ocean water, which are a few degrees Celsius warmer than the air and whose areas are of the order of 100 sq km, were the cause of the inversion rise.

In the late 1960's, Calspan studied Lake Effect snow storms which occur as cold air under a 1 km high inversion flows over one of the Great Lakes whose water is warmer than the air by 10-15°C and whose area is of the order of 500 sq km. As part of that study, Calspan (Eadie et al, 1971) utilized a numerical model (Lavoie, 1972) which simulated the rise in inversion height caused by perturbation vertical motions produced by the heating from the

lake. The similar scaling between the major parameters of the Lake Effect storms and the inversion rise fog type suggested using the Lavoie model to simulate that particular fog situation.

Phase I of this study, therefore, investigated the feasibility of applying the Lavoie model to the inversion rise fog type. Cases were selected in which the warm water patches were delineated in the DMSP IR data under clear skies and the cloud patterns were observed in subsequent DMSP visual data. For one case, whose synoptic situation fitted that which accompanies inversion rising fogs, the correspondence between predicted and observed small-scale cloud patterns was encouraging. For another case, the correspondence between cloud patterns was not as good because the accompnaying synoptic situation was that which produces a large-scale fog stratus system along the California coast.

With encouraging results from Phase I, Phase II of the program was undertaken to 1) further investigate the applicability of the Lavoie model to predicting fog/stratus in inversion rising situations; 2) incorporate long wave radiation into the model; and 3) perform a sensitivity analysis on the model. This report presents the results of Phase II and incorporates those parts of the Phase I technical report (Rogers and Hanley, 1979) which are required for this final report.

In Phase II, work was directed toward obtaining more information about the meteorology of the situation which was being simulated. Activity proceeded along two lines. One was a detailed case study of the 9 October 1976 situation, and the other was an attempt to find additional cases in satellite data archives. The archive search, following the guidelines used earlier for the DMSP data, was extended to the NOAA satellite data archives located at the Satellite Data Services in Washington, D.C. This search showed that in all cases for which satellite IR data were available under clear skies on one day, only large-scale stratus cloud systems occurred on the succeeding day. This result strongly suggested that the inversion rising fog situation occurred only rarely, or very rapidly.

In parallel with Phase II, Calspan personnel were working on a contract for NavAir 370 in which detailed investigations of the synoptic meteorology of fog episodes encountered on previous Calspan field trips were carried out. The case of 9 October 1976 was thoroughly investigated as part of both projects. Analysis showed that in about four hours the meteorological conditions went from clear skies with the inversion at 100m and below the LCL to cloudy skies with an inversion at 250m and above the LCL. During this time period the synoptic scale pattern at 850mb in the area changed from the center of a high pressure ridge to a col between high and low pressure pairs. The total inversion rise of 150m over four hours probably represents the change from a quasi-steady state associated with the ridge center to another quasi-steady state associated with the col.

In the first three hours when the inversion was rising above the LCL the inversion rise rate was 25m/hr. Numerical simulations with the Lavoie model suggest an inversion rise rate from warm patch effects of $\sim$5m/hr. Thus, only in the early stages when the inversion is just rising above the LCL does it appear that cloud could be produced only downstream from the warm patch. In a couple of hours the height rises from the changing synoptic scale flow pattern produces cloud over an area large compared to the warm patch area and overwhelms the effect of the warm patch on the inversion height and the cloud formation.

The above analysis indicates that the time period during which the warm patch primarily produces the cloud pattern is relatively short. In addition the results of the satellite search and synoptic climatology indicate that the frequency of occurrence of the inversion rising synoptic situation is small. These facts taken together strongly suggest that the absolute amount of time when the warm patch effect is important for stratus/fog formation is very small.

In summary, a modified numerical framework was constructed from the Lavoie model which is capable of simulating the effect of warm water patches on the formation of stratus/fog during inversion rising situations. However, we conclude that the operational utility of the model is limited because the frequency of conditions during which the warm patch effect is important is very small.

Section 2
FORMULATION OF THE LAVOIE MODEL

The Lavoie model consists of an upper and lower layer separated by an inversion whose height is H. The prognostic equations are applied to the well-mixed layer in which the wind, potential temperature and mixing ratio are vertically homogeneous. Potential temperature may vary vertically in the upper layer but the values remain fixed during the simulation. At the inversion, there is a discontinuity in potential temperature. The value at the base of the upper level, θ_L, is greater than θ in the mixed layer. At the top of the upper layer, Z, the potential temperature, θ_Z, may be equal to or different from θ_L. The difference between θ in the mixed layer and the mean temperature in the upper layer, $1/2\ (\theta_L + \theta_Z)$ governs the magnitude of the inversion height change produced in a simulation. The larger the θ-difference, the smaller the increase in inversion height.

In deriving an expression for the pressure gradient in the well-mixed layer, two non-perturbation terms appear which provide the large-scale pressure force: 1.) the pressure gradient at the top of the upper layer and 2.) the thermal wind in the upper layer. These parameters and the initial wind field specify the large-scale framework within which the wind perturbations arising from the warm patch are to occur. To focus simulations on the effects of these wind perturbations, the initial acceleration is required to be zero. Since both the initial wind and the large-scale pressure gradient are chosen to represent observed conditions, the thermal wind term must then be computed so that the initial acceleration is zero.

		Advective Term		Coriolis Term		Frictional Force		Large Scale Pressure Force	
$\frac{\partial u}{\partial t}$	=	$-\vec{V}\cdot\nabla u$	+	fv	-	$C_{DRAG}\lvert\vec{V}\rvert u$	-	$\frac{1}{\rho}\frac{\partial P}{\partial X}$	(1)

Perturbation Pressure Forces

	Inversion Height Deformation		Surface Heating
+	$\frac{g}{\theta_L}\left[\theta - \frac{\theta_L + \theta_Z}{2}\right]\frac{\partial H}{\partial X}$	+	$\frac{gH}{2\theta}\frac{\partial \theta}{\partial X}$

$$\frac{\partial v}{\partial t} = -\vec{V}\cdot\nabla v - fu - C_{DRAG}|\vec{V}|v - \frac{1}{\rho}\frac{\frac{2P}{2y}}{} + \frac{g}{\theta_L}\left[\theta - \frac{\theta_L + \theta_Z}{2}\right]\frac{\frac{2H}{2y}}{} + \frac{gH}{2\theta}\frac{\frac{2\theta}{2y}}{} \quad (2)$$

$$\frac{\partial \theta}{\partial t} = \underbrace{-\vec{V}\cdot\nabla\theta}_{\text{Advective Term}} + \underbrace{C_{HEAT}|\vec{V}|(\theta_{Surface} - \theta)}_{\text{Surface Heating}} \quad (3)$$

$$\frac{\partial H}{\partial t} = \underbrace{-\vec{V}\cdot\nabla H}_{\text{Advective Term}} - \underbrace{H\left(\frac{\partial u}{\partial x} + \frac{\partial v}{\partial y}\right)}_{\text{Vertical Velocity (Divergence) Term}} \quad (4)$$

Mathematically, the model has the form shown in Equations 1-4. Initially, the advection term equals zero in Equations 1 and 2 and the coriolis and frictional terms are specified by the initial velocity field. The direct surface heating, computed from Equation 3, stimulates localized pressure changes which produce acclerations (Equations 1 and 2) and a non-zero divergence field. The last term in Equation 4 is the vertical velocity at the inversion base, determined by the product of inversion height and divergence. This term causes a change in the inversion height and extends the pressure perturbation by altering the fraction of air beneath and above the inversion in the model. The inversion height deformation term is included in subsequent computations of acceleration in Equations 1 and 2.

2.1 Moisture

The prognostic equation for average water vapor content in the well-mixed layer which has been incorporated into the Lavoie model takes the form

$$\frac{\partial r}{\partial t} = -\vec{V}\cdot\nabla r + EVAP - \frac{COND}{\bar{\rho} H} \quad (5)$$

where r is the average mixing ratio for the layer, $\vec{V}$ is the horizontal wind vector, H is the height of the capping inversion surface or the thickness of the layer, and COND is the net condensation rate in a unit column of the layer of mean density $\bar{\rho}$. EVAP is a parameterization of evaporation from the water surface by the bulk aerodynamic method and is given by

$$EVAP = \frac{C_E \left|\vec{V}\right| (r_s - r)}{H} \tag{6}$$

where the surface mixing ratio r_s is assumed equal to the saturation mixing ratio at the ocean surface temperature, and C_E is a drag coefficient for evaporation assumed equal to a drag coefficient for exchange over the ocean.

The prognostic equation for the total mass of cloud water Q in a unit column of the layer is written

$$\frac{\partial Q}{\partial t} = \vec{V} \cdot \nabla Q + COND \tag{7}$$

Cloud liquid water content was computed by dividing Q by the cloud depth defined as inversion height minus lifting condensation level.

In addition, the potential temperature equation of the model was modified by addition of a term accounting for the release of latent heat of condensation. The potential temperature equation becomes

$$\frac{\partial \Theta}{\partial t} = -\vec{V} \cdot \nabla \Theta + \frac{C_H \left|\vec{V}\right| (\Theta_s - \Theta)}{H} + \frac{L}{C_p} COND \tag{8}$$

where Θ_s is the surface temperature, C_H is a drag coefficient for heat exchange, L is the latent heat of condensation, and C_p is specific heat of air at constant pressure.

The condensation rate in a unit column of the layer can be computed by assuming that liquid water is generated by the mesoscale updrafts

in a moist adiabatic process taking place between cloud base and the mean cloud tops at the capping inversion surface. This can be expressed mathematically as

$$COND = -\bar{\varrho} \int_C^H \frac{dr_s}{dz} \, WdZ \qquad (9)$$

where $\frac{dr_s}{dz}$ is the derivative of saturation mixing ratio r_s with height Z, $W = -Z\nabla\cdot V$ is the mesoscale vertical velocity predicted by the model, and C is the cloud base height or lifting condensation level computed from r and θ. If we now simplify the integral by assuming an appropriate mean value for $\frac{dr_s}{dz}$, we obtain

$$\begin{aligned} COND &= \bar{\varrho} \, \overline{\frac{dr_s}{dz}} \, \vec{\nabla}\cdot V \int_C^H Z dZ \\ &= \bar{\varrho} \, \overline{\frac{dr_s}{dz}} \, \nabla\cdot\vec{V} \left(\frac{H^2-C^2}{2}\right) \\ &= \bar{\varrho} \, \overline{\frac{dr_s}{dz}} \, W_H \left(\frac{H^2-C^2}{2H}\right) \end{aligned} \qquad (10)$$

where $W_H = -H\nabla\cdot\vec{V}$ is the vertical velocity at the inversion surface H.

This procedure for condensation produced very small maximum values of cloud liquid water, of the order of 0.05 g/m^3 primarily because of small vertical velocities. From our observations of marine fogs, we know that LWC should be at least 0.10 g/m^3 for young fogs and greater than that for stratus clouds. Therefore, a parameterization of condensation which had been used in application of the Lavoie model to Lake Effect snow storms to increase the condensation was used. This formulation was

$$COND = -\varrho r W_H. \qquad (11)$$

Comparison of (11) to (10) shows that the two are dimensionally equivalent. The values of cloud LWC computed from this formulation were too large, giving maximum values of 0.7 g/m^3 for a stratus cloud of ~100 m thickness.

Since incorporation of long-wave radiation into the model would have to be by parameterization based on LWC, an adequate and suitable determination of LWC was required. The condensation scheme used in Phase I had been designed to simulate the deep convective clouds of Lake Effect storms and was inappropriate for the shallow stratus cloud systems found off the west coast.

2.2 Modifications to the Lavoie Model

Recognition that we were dealing with a shallow, turbulent layer in which cloud forms as the air moves upward and evaporates as the air moves downward led to the following model framework. Cloud liquid water was diagnosed by assuming that cloud base was at the height of the LCL and that above the LCL the air followed the pseudo-adiabatic process to the height of the inversion. The total LWC of the cloud was taken as the difference between the mixing ratio at the LCL and that at the cloud top. The LWC values predicted by this scheme were of the proper magnitude, 0.1-0.3 g/m^3.

Within this cloud modeling framework, the mean potential temperature of the mixed layer, which is paramount in producing the perturbation accelerations in the wind field, is seen to be a layer weighted mean involving both the potential temperature below the cloud base (LCL) and the mean potential temperature in the cloud layer. The potential temperature below the cloud base was used to specify the temperature gradient between the air and the water, which drives the heat flux. This potential temperature was increased if the air was heated. Since the sub-cloud layer potential temperature is also the temperature at the base of the cloud, an increase in the sub-cloud layer temperature is transmitted to the mean cloud layer temperature. Thus, over a warm patch, the mean potential temperature of the mixed layer increases both from sensible heating of the entire layer and from the release of latent heat in the cloud.

The model uses a threshhold value of upward vertical motion to specify where cloud is present, and hence where the mean temperature is influenced by latent heat. Using a threshhold value attempts to model an effect of large-scale vertical motion on the mixed-layer cloud field, i.e., upward motion tends to increase while downward motion tends to decrease the fractional cloud cover in a volume.

Cloud Liquid Water

The model assumes that the potential temperature and mixing ratio are uniform from the surface up to cloud base and computes the lifting condensation level from the mixing ratio and potential temperature. The temperature at which the mixing ratio is the saturated value is computed and then the height of this temperature is computed from the dry adiabatic lapse rate. The pseudo-adiabatic process is assumed to operate at 0.5°C/100m from the LCL up to cloud top at the inversion height and the saturation mixing ratio at cloud top temperature is determined. The difference between the saturation mixing ratio at the cloud bottom and cloud top is then the total water content of the cloud; dividing by the cloud depth then provides the mean liquid water content of the cloud

Liquid water is diagnosed only at those grid points at which the vertical velocity is above a threshhold of +0.1 cm/sec. By requiring a positive value of vertical motion for the existence of cloud in the model, the model cloud pattern reflects the two-dimensional pattern of mesoscale vertical motion generated by the warm patch. The value of +0.1 cm/sec is arbitrary, but it is based on a qualitative assessment of the noise which is present in the vertical motion fields generated by the model.

Mean Layer Potential Temperature

With the above framework the mixed layer beneath the inversion is made up of a sub-cloud and cloud layer. The potential temperature and mixing ratio in the sub-cloud layer are what really drive this model. The perturbation

accelerations which disturb the inversion are caused primarily by heating of the mixed layer driven by the gradient in θ between the sub-cloud layer and the water in the warm patch. These temperature increases and moisture increases from evaporation determine the pattern of LCL height which is one effect on the cloud liquid water content pattern, the other being the pattern of inversion height deformation. The mesoscale vertical motion field generated by the perturbation accelerations determines 1.) where the cloud will be located through the 0.1 cm/sec threshhold and 2.) the pattern of the liquid water content as controlled by variations in cloud top height (inversion height).

With both a sub-cloud and a cloud layer present, the mean potential temperature in the acceleration equations must be a two-layer weighted mean temperature in which the cloud layer temperature reflects the release of latent heat. The cloud layer mean θ is determined using a 0.5°K per 100 m increase in potential temperature along the pseudo-adiabat.

New Model Equations

In this formalism, the equations of the model take the following form. Where cloud is present as determined by the 0.1 cm/sec vertical motion threshhold, θ in Eq (1) and (2) is the two-layer weighted mean. Outside the cloud area θ is the single, well-mixed layer θ. In Eq (3), θ is the well-mixed or sub-cloud layer θ, whichever is appropriate. In Eq (5), condensation is not considered a sink of vapor because of the diagnosis of liquid water content. Similarly, condensation is not a source of heat in Eq (8), this heat is taken account of in the computation of mean θ in cloudy areas. Equation 7 is elimated entirely, as are all equations dealing with the computation of condensation, since cloud water is diagnosed.

Upstream Evaporation

The cloud field in this model is controlled by both evaporation and inversion height change. Evaporation affects the magnitude of the LWC through lowering the LCL. Initial values of LCL above the inversion, required a

mixing ratio in the air which was less than that over the cold water. Evaporation then took place into the air as it moved toward the warm patch. The vertical motion threshhold for cloud formation was not exceeded until the air reached the warm patch. At this point, the cloud base was instantaneously lowered by evaporation which had been in operation for some time while only a relatively small increase in inversion height and cloud top occurred. Thus, evaporation having nothing to do with the warm patch, was dominating the cloud field. To insure that the model cloud reflected only the presence of the warm patch, upstream evaporation was eliminated by initializing the cold water temperature so that the cold water mixing ratio matched that in the air. This procedure usually produced a warm-water, cold-water temperature difference of 5°C, but the air-warm water temperature difference remained at 2°C, a value which corresponded to observations.

Section 3
RESULTS

3.1 Simulations as the Model Framework Evolved

It is instructive to compare the results of simulations as the modeling framework evolved and the input procedures were changed. Figure 1 shows the model cloud simulation after 12 hours along with the observed cloud pattern for the July 1977 case. The model framework used for this simulation is the one described above. The model diagnoses the liquid water content based on the 0.1 cm/sec vertical motion threshhold, this same threshhold is used in computing a two-layer mean temperature, and the cold water temperature is set to preclude evaporation upwind of the warm patch.

The correspondence between the simulated and observed cloud pattern is good. The shapes of the simulated 0.1 g/m^3 isopleth and the observed area of broken cloud are very similar. In fact, if the observed pattern is shifted 60 km to the west, the two patterns match extremely well. In view of the 36-hour difference between the observations of the warm patch and the cloud pattern and error in the geographical location of both the warm patch and the cloud pattern, the match is remarkable.

The evolution of the model framework can be seen by considering Figure 2 which shows the simulation obtained at the end of Phase I and the one obtained after the first improvement under Phase II, diagnosing LWC based on 0.0 cm/sec threshhold. The large liquid waters of the Phase I simulation have been eliminated but the cloud now extends a long way downstream from the upwind edge of the warm patch in response to the downstream extension of the vertical motion field.

Figure 3 compares simulations from this framework and one in which the two-layer mean temperature was computed only where cloud was diagnosed. The width of the cloud area shrinks a little bit as the vertical motion field shrinks, but the downwind elongation in the cloud pattern remains.

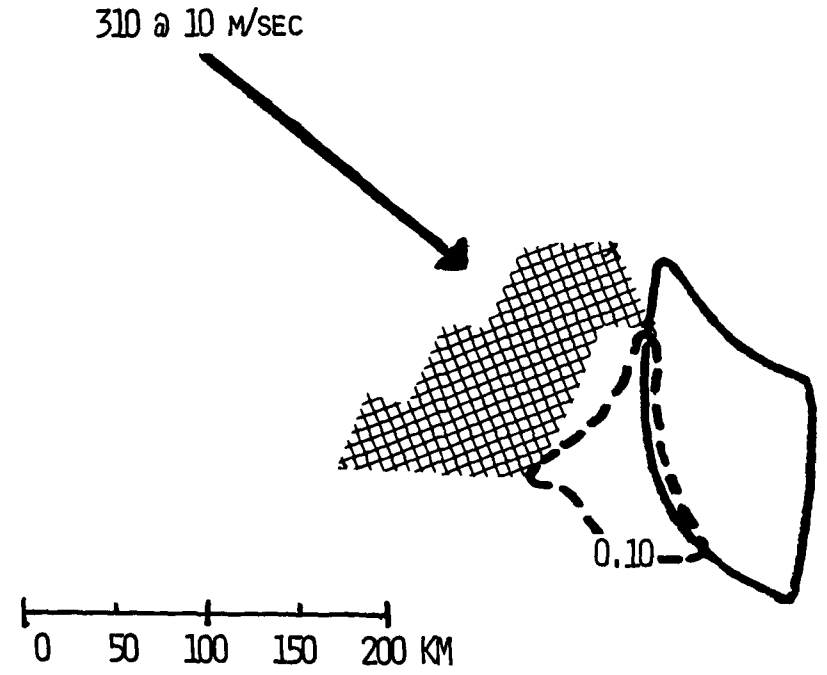

FIGURE 1 SIMULATED AND OBSERVED CLOUD PATTERNS, 5 - 6 JULY 1977

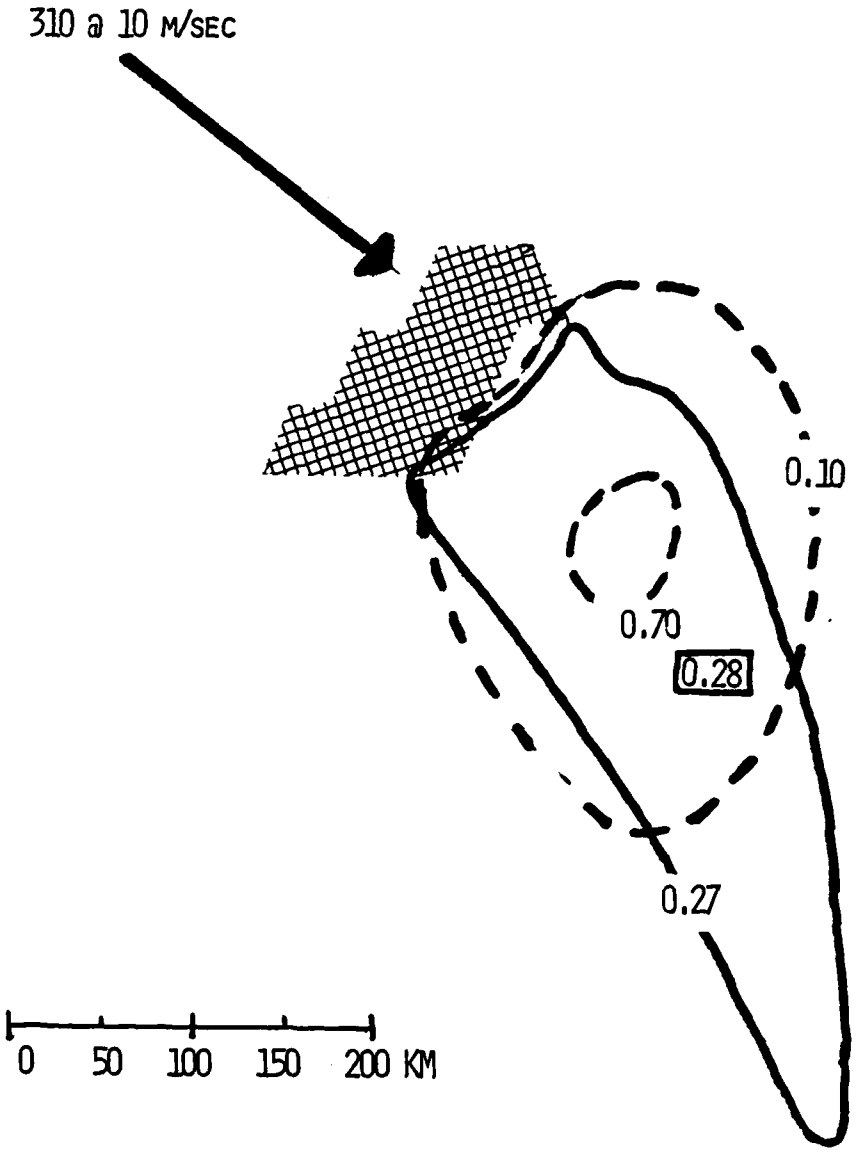

– – – – – SIMULATED CLOUD LWC(G/M^3) USING CONDENSATION COMPUTED FROM VERTICAL VELOCITY

——— SIMULATED CLOUD LWC(G/M^3) USING DIAGNOSIS OF VAPOR CHANGE ALONG SATURATED ADIABAT

FIGURE 2 COMPARISON OF SIMULATED CLOUD PATTERNS USING DIFFERENT CONDENSATION SCHEMES

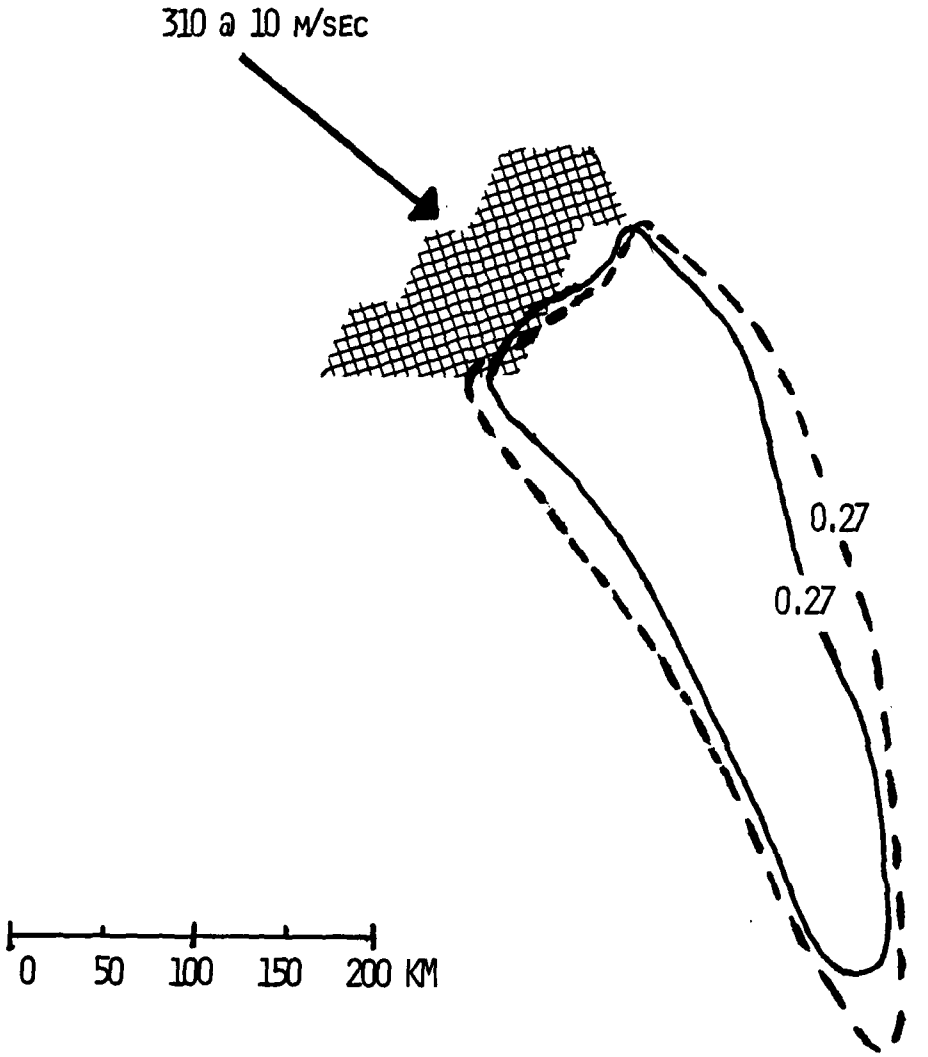

- - - - - SIMULATED CLOUD LWC(G/M^3) USING "TWO-LAYER" MEAN TEMPERATURE IN MIXED LAYER EVERYWHERE

_____ SIMULATED CLOUD LWC(G/M^3) USING "TWO-LAYER" MEAN TEMPERATURE IN MIXED LAYER IN CLOUD ONLY

MAXIMUM LWC IN BOTH CASES IS 0.28G/M^3

FIGURE 3 COMPARISON OF SIMULATED CLOUD PATTERNS USING MEAN TEMPERATURE EVERYWHERE AND IN CLOUD ONLY

Figure 4 compares the simulations between the new framework and the next improvement which was to eliminate evaporation over the cold water upwind of the warm patch. The downwind extension of the cloud pattern (the 0.10 g/m^3 isopleth) was reduced by 200 km.

The final change to the modeling framework was increasing the vertical motion threshhold from 0.0 to 0.1 cm/sec in an attempt to have the model cloud boundary better match the observed outer boundary of the broken cloud area. The effect of this change is seen in Figures 5 and 1. The area of the simulated cloud now becomes commensurate with the observed area, and except for the displacement of 60 km to the west, nearly matches the observed broken cloud area.

In summary, we have shown that the final modeling framework simulates the observed cloud pattern, although the effect of the mesoscale motion on the cloud amount and the effect of the reduction of evaporation over the cold water upwind of the warm patch are crudely handled.

3.2 Long Wave Radiation

Long wave radiation was introduced into the model via parameterization since this model has no vertical resolution. The parameterization assumes net long wave flux at cloud top when the cloud becomes radiationally opaque. Calspan observations in radiation fog at Travis AFB, CA (Mack and Pilie, 1973) suggested that with a total column liquid water of 4 g the fog behaved as a blackbody with the only region of net flux divergence located at fog top. Oliver et al (1978) substantiated this value of total cloud water in their simulations with a higher order closure model.

In the current model, radiational cooling is allowed to operate when the total cloud liquid water reaches the 4 g value. The cooling is computed by assuming the net flux is given by 25% of the black body flux at the cloud top temperature; this assumption allows for 75% back radiation from the sky. As with the heating from the surface, this cooling is applied to the sub-cloud layer potential temperature.

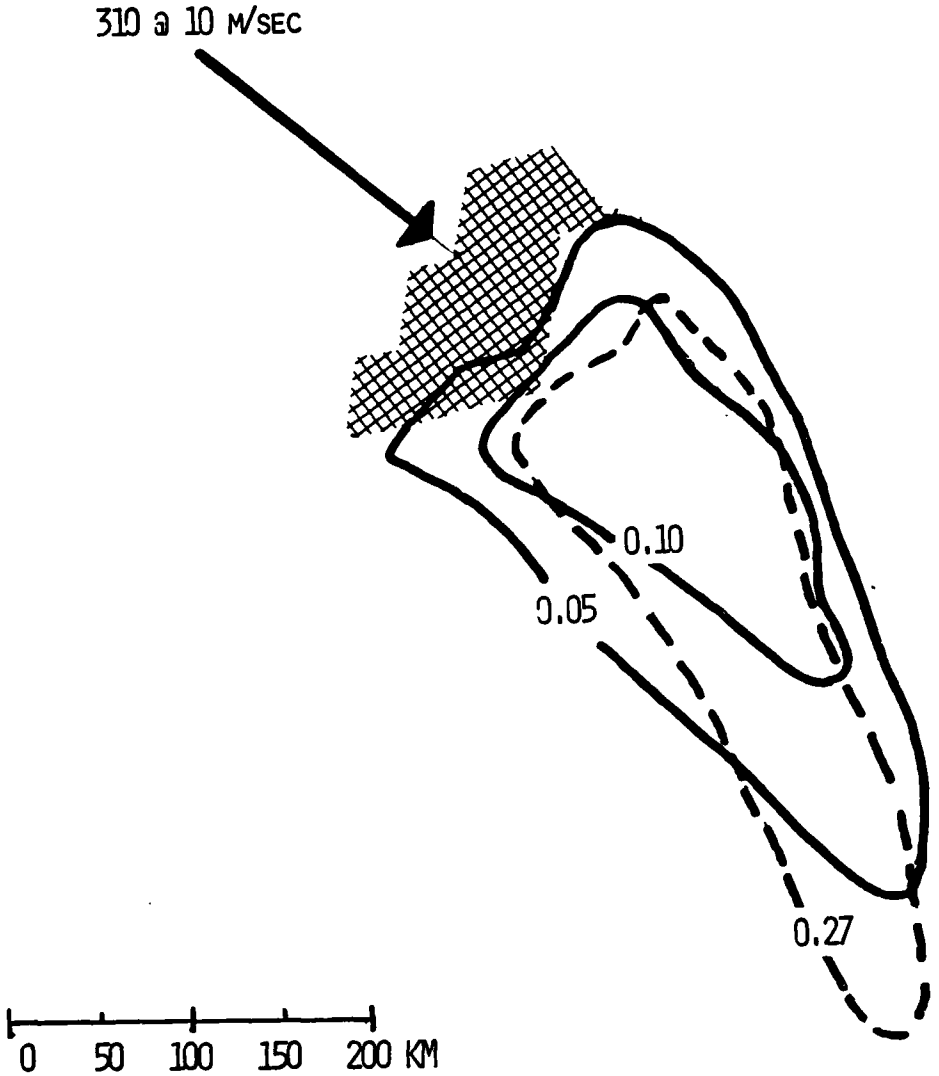

_ _ _ _ SIMULATED CLOUD LWC(G/M^3) WITH EVAPORATION FROM COLD WATER SURROUNDING WARM WATER PATCH

_____ SIMULATED CLOUD LWC(G/M^3) WITH NO EVAPORATION FROM COLD WATER SURROUNDING WARM WATER PATCH

FIGURE 4 COMPARISON OF SIMULATED CLOUD PATTERNS WITH AND WITHOUT EVAPORATION FROM COLD WATER SURROUNDING WARM PATCH

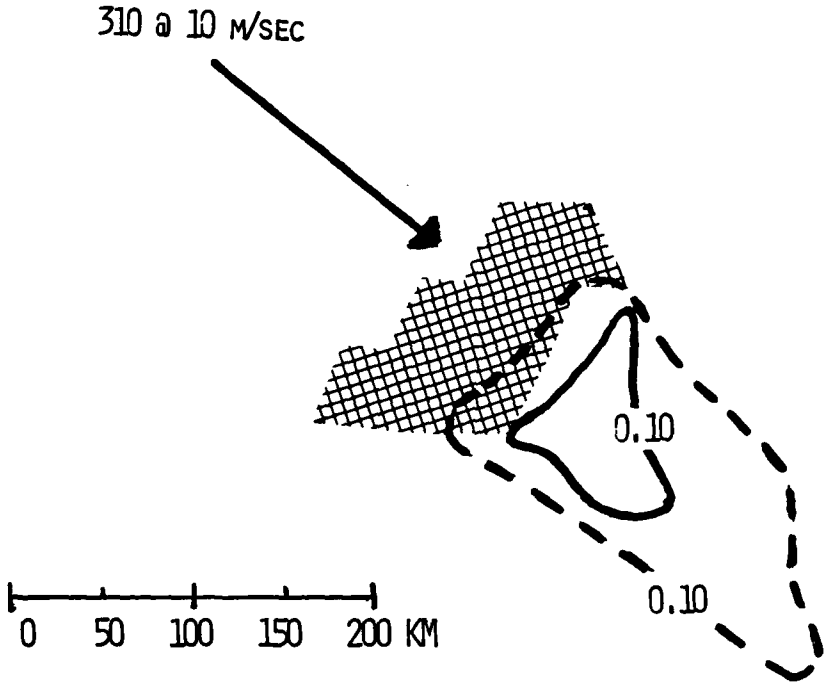

---- SIMULATED CLOUD LWC(G/M^3)-VERTICAL MOTION THRESHOLD FOR CLOUD DIAGNOSIS IS 0.0 CM/SEC

——— SIMULATED CLOUD LWC(G/M^3)-VERTICAL MOTION THRESHOLD FOR CLOUD DIAGNOSIS IS 0.1 CM/SEC

FIGURE 5 COMPARISON OF SIMULATED CLOUD PATTERNS USING DIFFERENT VERTICAL MOTION THRESHOLDS FOR DIAGNOSIS OF CLOUD

With radiation in the model, the maximum mean liquid water content of .12 g/m^3 for the July 1977 case increased by 0.003 g/m^3 which for the cloud depth of 33 m represents an increase of 0.10 g of total cloud water. The change in LWC was due to lowering of the LCL of a few meters by radiational cooling, since the mixing ratio in the sub-cloud layer did not change between the simulations. Although the radiation parameterization in the model is crude, it does produce the observed effect of lowering the cloud base.

Section 4
SENSITIVITY ANALYSIS

In the sensitivity analysis, initial and boundary conditions were varied in order to study the response of the Lavoie model to measurement errors in the input quantities. The parameters which were varied were:

1. Initial wind speed and direction
2. Initial inversion height
3. Temperature of warm water patch relative to initial air temperature
4. Initial lifting condensation level which depends primarily on initial air mixing ratio
5. Temperature of the cold water which controls evaporation upwind of the warm patch.

A wind range of values was not used to test each variable and, therefore, tables of output variables vs input parameters are not presented. However, the comparison among a few simulations permits an assessment of the variability in results produced by changing an initial or boundary parameter. All comparisons presented here are for steady state conditions.

4.1 Wind Speed

Since this model uses bulk equations for heat and moisture flux at the ocean surface, the transfer rates are directly proportional to wind speed. The maximum values of temperature and mixing ratio, which depend on the surface flux do not change magnitude or location as the wind speed is changed; rather, the time into the simulation at which these parameters reach a given value changes. For example, halving the wind speed halves the transfer rates, but the air takes twice as long to traverse a given distance so that the total transfer is equal in the two cases. It just takes twice as long to accomplish the transfer in the slower speed case.

A change in wind speed also causes a rotation of the major axis of the disturbance generated by the warm patch. Figure 6 shows the 0.10 g/m^3 LWC isopleth (used in all the subsequent figures) from simulations in which the wind speed was 5 and 10 m/sec. Notice that the major axis for the lower wind speed case is rotated clockwise relative to that for the higher wind speed case. This difference lies in the effect of the perturbation acceleration field on the initial wind.

In the early portion of the simulation, the perturbation acceleration field depends primarily on the heating and is essentially the same in both cases. For the lower wind speed, this acceleration produces a greater wind direction change and hence the larger rotation of the axis for the lower wind speed.

4.2 Wind Direction

Figure 7 shows the two cloud LWC isopleths obtained when the initial wind direction differed by 20°. The angular rotation between the major axes of the patterns is 20°, the same as the change in initial wind direction.

An interesting difference between these two patterns is that the more clockwise pattern (Case 2) is somewhat narrower and extends farther downstream from the warm patch. In Case 2, the residence time of the air over the warm patch is longer. The vertical motion field (not shown) is stronger in Case 2, reflecting the increased intensity of the disturbance generated as the warm patch affects the air longer.

The shape and orientation of the warm patch affects the resultant cloud pattern. As seen in Figure 7, a 20° rotation in warm patch orientation changes both the shape and extent of the cloud pattern. The amount of the effect obviously depends on the axial symmetry of the warm patch. Orientation of long, narrow patches relative to the wind direction will affect the cloud pattern more than patches which are more nearly circular.

Figure 8 shows the effect of a 20° difference in wind direction when the wind speed is smaller. Again, the angle between the two patterns reflects the angle between the initial wind directions.

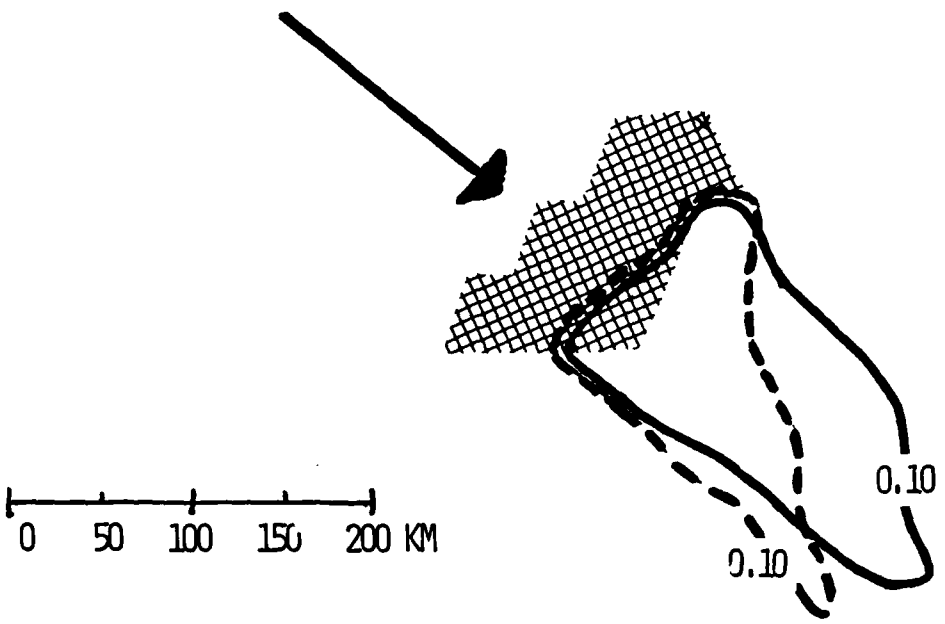

_____ SIMULATED CLOUD LWC(G/M^3)-INITIAL WIND SPEED OF 10M/SEC

- - - - SIMULATED CLOUD LWC(G/M^3)-INITIAL WIND SPEED OF 5M/SEC

FIGURE 6 COMPARISON OF SIMULATED CLOUD PATTERNS WITH DIFFERENT WIND SPEEDS

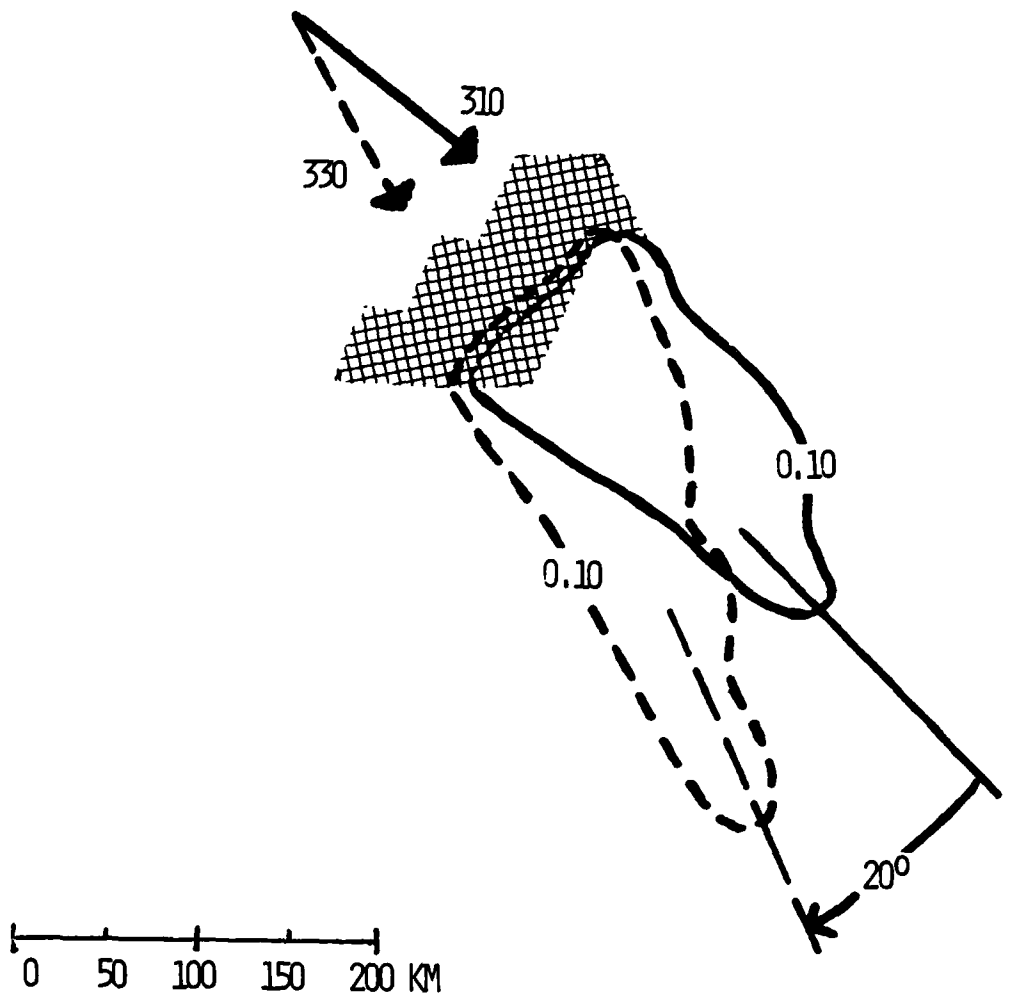

_____ SIMULATED CLOUD LWC(G/M^3)-310° WIND DIRECTION

_ _ _ SIMULATED CLOUD LWC(G/M^3) 330° WIND DIRECTION

FIGURE 7 COMPARISON OF SIMULATED CLOUD PATTERNS FOR DIFFERENT INITIAL WIND DIRECTIONS AT 10 M/SEC SPEED

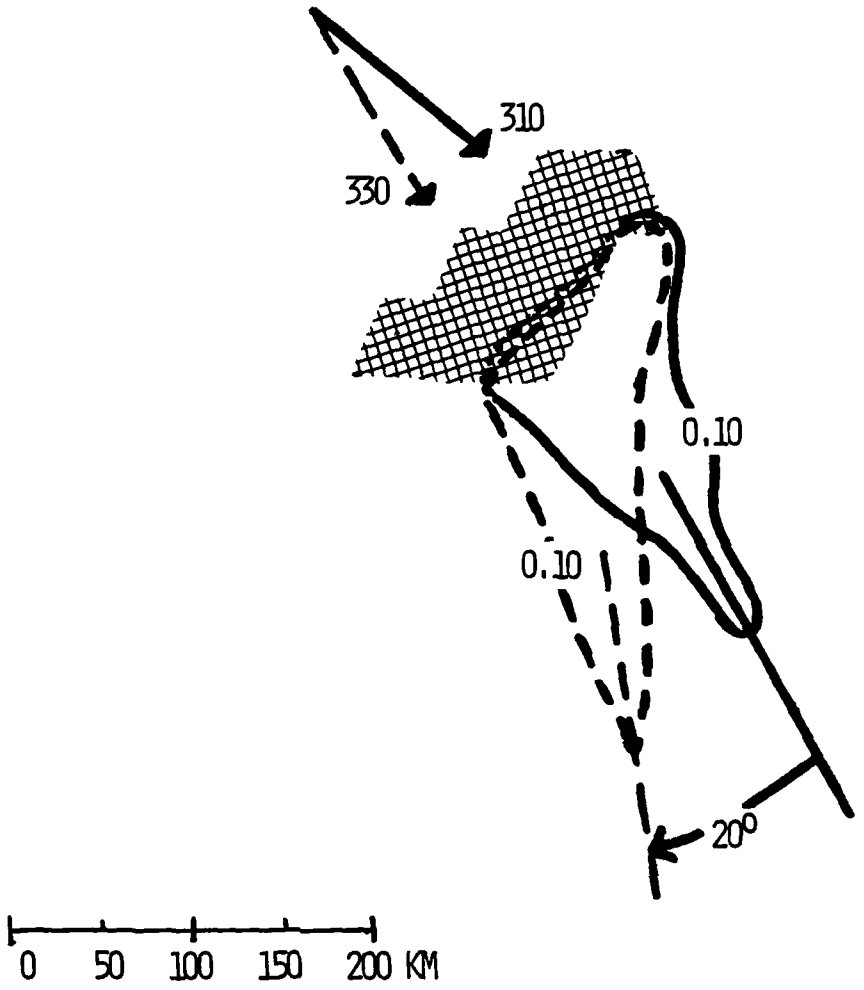

FIGURE 8 COMPARISON OF SIMULATED CLOUD PATTERNS FOR DIFFERENT INITIAL WIND DIRECTIONS AT 5 M/SEC SPEED

4.3 Change in Initial Inversion Height

Changes in initial inversion height change the magnitude of heating and mixing ratio increase, since in the mixed layer model any flux into the layer is distributed uniformly throughout the layer. Thus, the shallower the layer, the higher the heating and the larger the increase in mixing ratio. Since the inversion height is changed by the vertical velocity, whose magnitude depends on the layer divergence multiplied by the inversion, the inversion height increase is directly related to the initial inversion height. This relationship is not linear. As the simulation proceeds there is feedback since the higher the inversion rises, the larger the inversion change is for the same divergence field.

Before preceeding to the comparison of the various simulations, we present a list of the quantities whose initial or maximun, steady-state values appear in the following tables:

Initial Inversion Height - HI (meters)
Inversion Height Change - ΔH (meters)
Initial Lifting Condensation Level - CI (meters)
Lifting Condensation Level - LCL (meters)
Air Temperature Change - ΔT (°C)
Initial Mixing Ratio - RI (g/kg)
Mixing Ratio Change - ΔR (g/kg)
Saturation Mixing Ratio at Cold Water Temperature - R_C (g/kg)
Mean Cloud Liquid Water Content - LWC (g/m^3)
Divergence of Mixed-Layer Wind Field - DIV ($x10^{-6}$ sec^{-1})
Vertical Velocity - W (cm/sec)
Warm Water-Air Temperature Difference - TDELT (°C)
Initial Wind Speed - VI (m/sec)
Model Inversion Strength - $(\Theta_L - \Theta)$ (°K)

Unless otherwise indicated, the values used in the simulations are:

TDELT = 2°K
VI = 10 m/sec

Air Temperature = 285°K

RI = 7.3 g/kg

R_C = 8.9 g/kg

$\Theta_L - \Theta$ = 1°K

Table 1 shows the maximum values of simulated quantities as a function of initial inversion height. The increase in temperature and mixing ratio is larger for the shallower layer. The inversion height increase (ΔH) is larger in the higher inversion case which reflects the larger vertical velocity driving the inversion change. The non-linearity in ΔH vs HI shows up with a 1.5 times higher inversion providing an almost three times larger ΔH. The LWC is greater in the higher inversion case primarily as a result of the higher inversion and cloud top. The convergence is greater in the higher inversion case probably because the inversion deforms more and the perturbations in the wind field are larger.

Table 1

COMPARISON OF SIMULATIONS WITH DIFFERENT INITIAL INVERSION HEIGHTS

HI	ΔH	ΔT	ΔR	LCL	LWC	DIV	W
300	50	0.8	1.67	5	.34	-12	0.4
200	18	1.0	1.90	0	.22	-9	0.2

The above comparison was for two cases in which the initial inversion height was the only parameter which was changed between the two simulations. We now compare two simulations in which the initial lifting condensation level, along with the inversion height, was different. Table 2 shows the comparison between these two simulations. This table has added to it the initial mixing ratio of the air. Comparison of the second line of Tables 1 and 2 shows that the only variable affected by the higher mixing ratio is the increase in mixing ratio which is less since the gradient between air and water mixing ratio is less.

Table 2

COMPARISON OF SIMULATIONS WITH DIFFERENT INITIAL LIFTING CONDENSATION LEVELS

HI	CI	RI	ΔH	ΔT	ΔR	LCL	DIV	W
300	310	7.3	50	0.8	1.67	5	-12	0.4
200	210	7.7	18	1.0	1.51	0	-9	0.2

4.4 Different Warm Water Temperatures

Table 3 shows the maximum output values for simulations which used air-water temperature differences of 2 and 4°C, respectively. Doubling the temperature difference doubles the temperature increase in the air. The non-linearity of the model again shows up as doubling the temperature difference almost triples the inversion height increase. The divergence also increases non-linearly. The temperature increase doubles in direct proportion to the doubling of the difference between the warm patch temperature and the air temperature. The mixing ratio change increases by 30% in proportion to the change in mixing ratio over the warm water.

Table 3

COMPARISON OF SIMULATIONS WITH DIFFERENT WARM PATCH TEMPERATURES

HI	TDELT	ΔH	ΔT	ΔR	LCL	LWC	DIV	W
300	2	28	0.8	1.62	36	.31	-10	0.3
300	4	80	1.6	2.14	24	.38	-29	1.1

Notice the small change in lifting condensation level between the two simulations. This change is the net result of two competing influences. The warmer temperature raises the inversion while the increased mixing ratio lowers it; the net result in this case is to lower it slightly.

4.5 Different Wind Speed

Table 4 shows maximum output values for two simulations in which the wind speed was different. Values for the slower speed case are for a simulation run for twice as long as the higher speed case. Differences occur in the parameters related to the wind perturbations. As mentioned in the earlier discussions, the initial accelerations are roughly the same so that the weaker wind speed experiences larger relative acceleration and larger perturbation winds. Therefore, the divergence, vertical velocity, and ΔH are larger. The larger ΔH is reflected in the slightly larger liquid water content in the slower wind speed case.

Table 4

COMPARISON OF SIMULATIONS WITH DIFFERENT INITIAL WIND SPEED

VI	HI	ΔH	ΔT	ΔR	LCL	LWC	DIV	W
10	300	15	0.8	.99	168	.13	-4	0.1
5	300	31	0.8	.99	168	.14	-9	0.3

4.6 Different Lifting Condensation Level

Table 5 shows the effect of a different lifting condensation level which is related to the difference in air mixing ratio. The only difference is the increase in mixing ratio change which is directly related to the increased gradient in mixing ratio between the air and the ocean.

Table 5

COMPARISON OF SIMULATIONS WITH DIFFERENT INITIAL CONDENSATION LEVEL ONLY

CI	RI	HI	ΔH	ΔT	ΔR	LCL	LWC	DIV	W
210	7.7	200	18	1.0	1.50	6	.22	-9	0.2
310	7.3	200	18	1.0	1.88	9	.21	-9	0.2

4.7 Elimination of Upstream Evaporation

As mentioned earlier, one of the problems encountered in these simulations was with the evaporation from the cold water upwind of the warm patch. The procedure used to eliminate that effect was to lower the cold water temperature such that its saturation mixing ratio was equal to or less than the initial mixing ratio in the air. Table 6 shows the effect of this procedure on the simulations. As in the previous section, only those variables directly related to the moisture are affected by this change. The LCL is higher and the ΔR is lower when the evaporation upwind of the warm patch is eliminated. Similarly, the cloud liquid water is smaller since the LCL is higher.

Table 6

COMPARISON OF SIMULATIONS WITH DIFFERENT COLD WATER TEMPERATURES

RC	RI	HI	ΔH	ΔT	ΔR	LCL	LWC	DIV	W
8.88	7.30	300	28	0.8	1.67	11	.31	-10	0.3
7.30	7.30	300	28	0.8	1.01	.65	.15	-10	0.3

4.8 Different Inversion Strength in the Model

Table 7 shows the results of two simulations in which the inversion strength in the model was changed from 1 to 3°C. The only difference is a very slight decrease in ΔH for the more stable, stronger inversion case.

Table 7

COMPARISON OF SIMULATIONS WITH DIFFERENT INVERSION STRENGTH

$\theta_L - \theta$	HI	ΔH	ΔT	ΔR	LCL	LWC	DIV	W
1	300	20	0.8	1.60	31	.28	-6	0.2
3	300	17	0.8	1.60	31	.28	-6	0.2

REFERENCES

1. Eadie, W.J., U. Katz and C.W. Rogers, 1971: Investigations of Lake-Effect Snowstorms, Final Report on Contract No. E22-59-71(N), 29 November 1971. CAL Report No. VC-3034-M-1, Cornell Aeronautical Laboratory, Inc., Buffalo, NY.

2. Lavoie, R.L., 1972: A Mesoscale Numerical Model of Lake Effect Storms, J. Atmos. Sci., 29, 1025-1040.

3. Mack, E.J. and R.J. Pilié, 1973: The Microstructure of Radiation Fog at Travis Air Force Base. Final Report on Contract No. F19628-72-C-0160, Calspan Report No. CJ-5076-M-2, September 1973, 63 pp.

4. Oliver, D.A., W.S. Lewellen and G.G. Williamson, 1978: The Interaction Between Turbulent and Radiative Transport in the Development of Fog and Low-Level Stratus, J. Atmos. Sci., 35, 301-316.

5. Rogers, C.W. and J.T. Hanley, 1979: "Deformations of the Marine Inversions and the Development of Marine Fog and Stratus Resulting from Warm Water Patches: Numerical Modeling and Verifications with Satellite Imagery, Calspan Report No. 6512-M-1, November, 27 pp.